

## Initial condition from the shadowed Glauber model

Sandeep Chatterjee,\* Sushant K. Singh,† Snigdha Ghosh, Md Hasanujjaman, Jane Alam, and Sourav Sarkar  
*Theoretical Physics Division, Variable Energy Cyclotron Centre, 1/AF Bidhannagar, Kolkata, 700064, India*

### Abstract

The two component Monte-Carlo Glauber model predicts a knee-like structure in the centrality dependence of elliptic flow  $v_2$  in Uranium+Uranium collisions at  $\sqrt{s_{NN}} = 193$  GeV. It also produces a strong anti-correlation between  $v_2$  and  $dN_{ch}/dy$  in the case of top ZDC events. However, none of these features have been observed in data. We address these discrepancies by including the effect of nucleon shadowing to the two component Monte-Carlo Glauber model. Apart from addressing successfully the above issues, we find that the nucleon shadow suppresses the event by event fluctuation of various quantities, e.g.  $\varepsilon_2$  which is in accordance with expectation from the dynamical models of initial condition based on gluon saturation physics.

One of the major challenges in heavy ion collision (HIC) experiments is to comprehend the initial condition (IC). This is an essential requirement to extract crucial physical properties of the quark gluon plasma (QGP) phase e.g. the equation of state, the transport coefficients, etc. Studies suggest that the largest uncertainties on the extracted value of the ratio of the shear viscosity over entropy density arise from the ignorance of the IC [1].

Currently, two types of IC models are available. The first is the Monte-Carlo Glauber model (MCGM), a geometry based model of the initial distribution of the energy deposited in the transverse plane (with respect to the beam axis) [2–5]. The dynamical input is restricted to the constant nucleon-nucleon cross section  $\sigma_{NN}$  at given beam energy. This simple model has been fairly successful in providing the centrality dependence of various global observables. The second type of models which attempt to generate ICs are based on QCD [6–9]. A few of the recent successful approaches are color glass condensate based IP-Glasma model [10] and NLO pQCD and gluon saturation based EKRT model [11].

The recent data from STAR on U+U [12] and LHC on Pb+Pb [13, 14] have rung the death bell for the MCGM. The prolate shape of the U nucleus implies a knee-like structure in the centrality dependence of elliptic flow  $v_2$  [15, 16]. For the same reason, a strong anti-correlation is expected between  $v_2$  and multiplicity in the top zero degree calorimeter (ZDC) events [17]. However, none of these unique predictions of the two-component MCGM were seen in the data [12]. Moreover, MCGM predicts a broader event by event (E/E) distribution of flow observables  $v_n$  than seen in experiments [10, 11]. These observations tend to rule out the two component MCGM as a viable candidate to provide IC in HIC. On the other hand, the predictions from the dynamical models are in agreement with data [10, 11]. There have been several attempts to revive the Glauber model. The absence of knee

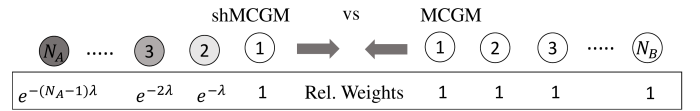


FIG. 1. The relative weight factors of each participant for energy deposition in the shMCGM (left) vs MCGM (right) for the simple case of collision between two rows with  $N_A$  (right going) and  $N_B$  (left going) number of nucleons in each.

in the centrality dependence of  $v_2$  in U+U could be explained by introducing fluctuating weight factors for the energy depositing sources [18]. The constituent quark model using wounded constituent quarks as sources for energy deposition is in agreement with the U+U data on  $v_2$  [12, 19, 20]. In Ref. [21], the simple two component scheme was replaced by a reduced nuclear thickness function that yielded results in better agreement with data. The simplicity of the two component MCGM approach is appealing as well as computationally cheap to implement. Therefore, it is an interesting question to ask whether to give up this geometrical idea altogether is the only way to make peace with the current data.

In the Eikonal limit the collisions of nucleon rows form the basis of MCGM. Fig. 1 illustrates such a scenario. As shown in the right hand side of Fig. 1, we note that in a MCGM approach all the nucleons that contribute to energy deposition are treated democratically and hence receive the same relative weight for energy deposition. Here we modify this approach by not treating all the participants and binary collisions identically - *the contribution to energy deposition by nucleons seated deep inside the nucleus is shadowed by those leading in front*. We call this the shadowed Monte Carlo Glauber Model (shMCGM). We use a simple suppression factor  $\mathcal{S}(n, \lambda)$  for the contribution from a nucleon which finds  $n$  other participants from the same nucleus ahead of it

$$\mathcal{S}(n, \lambda) = e^{-n\lambda} \quad (1)$$

where  $\lambda$  is a phenomenological parameter that is to be extracted from experiments. The modified weight factors in case of shMCGM in the simple case of a row on row

\* sandeepc@vecc.gov.in

† sushantsk@vecc.gov.in

collision is illustrated on the left hand side of Fig. 1. This idea of shadowing of nucleons by other nucleons inside a nucleus was first discussed about sixty years back [22]. However, barring a few studies [23], it has been rarely applied in the context of HICs. Here, we implement this scheme in nuclear collisions at relativistic energies for the first time within a Monte-Carlo approach. Our results indicate that nucleon shadowing in HICs has crucial consequences on several observables.

We will now discuss the details of the Glauber model. The nucleus is first constructed by generating the nucleons sampled from a Woods-Saxon profile. The  $i$ th nucleon from nucleus A with transverse coordinates  $(x_i^A, y_i^A)$  is made to undergo a binary collision with the  $j$ th nucleon from nucleus B with transverse coordinates  $(x_j^B, y_j^B)$  when their squared transverse separation  $\rho_{ij}^{AB}$  satisfy the following geometrical criteria

$$\rho_{ij}^{AB} \leq \frac{\sigma_{NN}}{\pi} \quad (2)$$

where  $\rho_{ij}^{AB}$  is defined as

$$\rho_{ij}^{AB} = (x_i^A - x_j^B)^2 + (y_i^A - y_j^B)^2 \quad (3)$$

Those nucleons from the colliding nuclei whose transverse coordinates satisfy Eq. 2 are identified as participants. The sum of the number of participants,  $N_{part}$  and all the possible binary collisions between them,  $N_{coll}$  give us the number of energy depositing and particle producing sources in an event in the Glauber model. The charged particle multiplicity at mid-rapidity  $dN_{ch}/dy|_{y=0}$  (henceforth we will drop the subscript  $y=0$  and refer to it by just  $dN_{ch}/dy$ ) in an event is expressed as a sum over all these sources with participant and collision sources receiving different weight factors parametrised by the hardness factor  $f$  as follows:

$$dN_{ch}/dy = \frac{(1-f)}{2} \sum_i^{N_{part}} w_i + f \sum_i^{N_{coll}} w_i \quad (4)$$

where  $w_i$  is source weight factor. In the simplest case it can be just taken as a constant  $n_0$  equal to the average  $dN_{ch}/dy$  for p-p collision. However, multiplicity distribution data in p-p and p-A show that the data is best described by sampling  $w_i$ s from a negative binomial distribution (NBD)  $P_{NBD}(w, n_0, k)$  with mean  $n_0$  and variance  $\sim \frac{1}{k}$  [24]

$$P_{NBD}(w, n_0, k) = \frac{\Gamma(k+w)}{\Gamma(k)\Gamma(w+1)} \frac{n_0^w k^k}{(n_0+k)^{w+k}} \quad (5)$$

In this work we follow the same strategy and consider NBD fluctuations in the  $w_i$ s to generate multiplicity. The energy deposition ansatz is also similar to Eq. 4. However, for the energy deposition scheme we have not considered any additional fluctuation as in Ref. [24] and just

considered  $w_i = \epsilon_0$ , a constant. We will now turn our discussion towards shMCGM. The only modification that is made to the above framework to obtain shMCGM is in Eq. 4 where there are now additional weight factors  $\mathcal{S}(n_i, \lambda)$  defined in Eq. 1 due to shadowing.  $n_i$  depends on whether the source is a participant or a binary collision: in case of a participant source it is equal to the number of nucleons that shadow it and in case of a binary collision it is the sum of the number of nucleons that shadow the two participants of the given binary collision.

We will now first try to understand the effect of introducing shadowing in shMCGM on observables computed thereof qualitatively neglecting the NBD fluctuations of the sources before discussing the Monte-Carlo results. Let us consider two nuclei A and B approaching each other along the z axis with the origin at the center of mass of the two nuclei system. As discussed earlier, the contribution to energy deposition due to a participant nucleon  $i$  from the nucleus A at  $(x_A^i, y_A^i, z_A^i)$  in the two-component scheme occurs through the participant term  $N_{i_{part}}^{sh}$  and collision term  $N_{i_{coll}}^{sh}$  which are obtained as follows

$$n(x_A^i, y_A^i, z_A^i) = \sum_{j=1, j \neq i}^{N_A} \Theta\left(\frac{\sigma_{NN}}{\pi} - \rho_{ij}^{AA}\right) \times \Theta\left(|z_A^i| - |z_A^j|\right) \quad (6)$$

$$m(x_A^i, y_A^i, z_A^i) = \sum_{j=1}^{N_B} \Theta\left(\frac{\sigma_{NN}}{\pi} - \rho_{ij}^{AB}\right) \quad (7)$$

$$N_{i_{part}}^{sh}(x_A^i, y_A^i, z_A^i, \lambda) = \mathcal{S}(n, \lambda) \quad (8)$$

$$N_{i_{coll}}^{sh}(x_A^i, y_A^i, z_A^i, \lambda) = \mathcal{S}(n, \lambda) \sum_{j=0}^{m-1} \mathcal{S}(j, \lambda) \quad (9)$$

Here  $\Theta(x) = 1$  for  $x \geq 0$  and 0 for  $x < 0$ .  $n$  has been already introduced in Eq. 1 and  $m$  is the number of nucleons from nucleus B with which the  $i$ th nucleon from nucleus A collides.

In order to understand the nucleon shadowing effect we will now focus on our earlier simple case illustrated in Fig. 1. Here

$$N_{part} = N_A + N_B \quad (10)$$

$$N_{coll} = N_A N_B \quad (11)$$

$$N_{part}^{sh} = \sum_{i=0}^{N_A-1} \mathcal{S}(i, \lambda) + \sum_{i=0}^{N_B-1} \mathcal{S}(i, \lambda) = \frac{2 - e^{-\lambda N_A} - e^{-\lambda N_B}}{1 - e^{-\lambda}} \quad (12)$$

$$N_{coll}^{sh} = \frac{1 - e^{-\lambda N_A} - e^{-\lambda N_B} + e^{-\lambda(N_A+N_B)}}{(1 - e^{-\lambda})^2} \quad (13)$$

The source for the E/E fluctuations in the MCGM ICs lie in the E/E fluctuations of the positions of the nucle-

ons sampled from the Woods-Saxon profile of the nucleus which in this case translate into fluctuation in  $N_A(x, y)$  and  $N_B(x, y)$

$$\delta N_{part} = \delta N_A + \delta N_B \quad (14)$$

$$\delta N_{coll} = N_B \delta N_A + N_A \delta N_B \quad (15)$$

$$\delta N_{part}^{sh} = \frac{\lambda}{1 - e^{-\lambda}} (e^{-\lambda N_A} \delta N_A + e^{-\lambda N_B} \delta N_B) \quad (16)$$

$$\delta N_{coll}^{sh} = \frac{\lambda}{(1 - e^{-\lambda})^2} ((1 - e^{-\lambda N_B}) e^{-\lambda N_A} \delta N_A + (1 - e^{-\lambda N_A}) e^{-\lambda N_B} \delta N_B) \quad (17)$$

As seen from Eqs. 12, 13, 16 and 17 in the  $\lambda \rightarrow \infty$  limit,  $N_{part}^{sh} \rightarrow 2$ ,  $N_{coll}^{sh} \rightarrow 1$  while their fluctuation is completely suppressed, thus in this limit the energy is deposited by the leading nucleons alone, irrespective of the number of nucleons present in the colliding rows. However, as it turns out from fits to data, the more relevant case is the  $\lambda \rightarrow 0$  limit. With  $N_A \sim N_B \sim N$ ,  $\delta N_A \sim \delta N_B \sim \delta N$  and  $(\lambda, \lambda N) \ll 1$ , we get

$$N_{part}^{sh} \simeq \left(1 - \frac{(N-1)}{2} \lambda\right) N_{part} \quad (18)$$

$$N_{coll}^{sh} \simeq (1 - (N-1)\lambda) N_{coll} \quad (19)$$

$$\delta N_X^{sh} \simeq (1 - N\lambda) \delta N_X \quad (20)$$

where  $N_X = (N_{part}, N_{coll})$ . Thus the shadow effect is expected to suppress the energy deposited as well as the E/E fluctuations of observables.

We will now report our findings. In this work we use the same Woods-Saxon parameters for U and deformed Au as used in Ref. [17]. The parameters of the MCGM as well as shMCGM are fixed by comparing the variation of the probability distribution for multiplicity,  $P(dN_{ch}/dy)$  with  $dN_{ch}/dy$  to that of IP-Glasma [17] as shown in Fig. 2. The values of the parameters used in this work are mentioned in Table I. From MCGM to shMCGM, the nucleon shadow effect in energy deposition is compensated by increasing the value of  $n_0$  and  $f$ . The fits to multiplicity distribution in p-Pb collisions at  $\sqrt{s_{NN}} = 5.02$  TeV yield  $k \sim 1$  [24]. In this work, we have taken  $k = 1.1$ .

We also compute the eccentricities of the initial energy density deposited that are expected to drive the momentum anisotropies of the produced particles measured in

Model	system	$n_0$	$k$	$f$	$\lambda$
MCGM	Au+Au	2.37	1.1	0.14	-
MCGM	U+U	2.30	1.1	0.14	-
shMCGM	Au+Au	2.83	1.1	0.32	0.12
shMCGM	U+U	2.83	1.1	0.32	0.12

TABLE I. The values of the parameters of the Glauber model used in this work. The results from a detailed fit procedure with allowed range in the parameter space will be reported elsewhere.

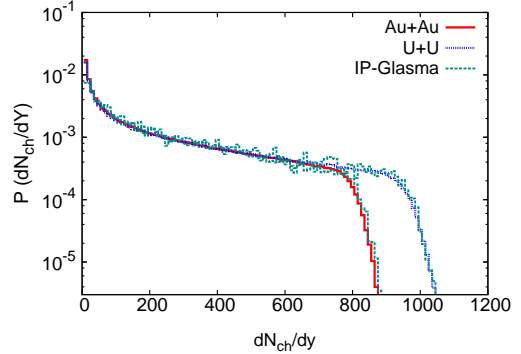


FIG. 2. The multiplicity distribution plot for U+U at  $\sqrt{s_{NN}} = 193$  GeV and Au+Au at  $\sqrt{s_{NN}} = 200$  GeV in shMCGM. The IP-Glasma data is from Ref. [17].

experiments. The standard way to compute the eccentricities  $\varepsilon_n$  of the overlap region is

$$\varepsilon_n e^{i\Psi_n} = \frac{\langle r^n e^{in\phi_n} \rangle}{\langle r^n \rangle} \quad (21)$$

where the averages  $\langle \dots \rangle$  are taken with the initial energy distribution on the transverse plane  $\epsilon(x, y)$  as the weight function. The energy  $\epsilon_i(x, y)$  deposited by the  $i$ th source of strength  $\epsilon_0$  located at  $(x_i, y_i)$  is smeared by a Gaussian profile

$$\epsilon_i(x, y) = \frac{\epsilon_0}{2\pi\sigma^2} e^{-\frac{(x-x_i)^2 + (y-y_i)^2}{2\sigma^2}} \quad (22)$$

where we have set the width  $\sigma = 0.6$  fm.

The full overlap U+U collision configurations can be of two types: (i) Body-Body (BB)- in this case the U nuclei approach each other along their minor axes and the overlap region has higher ellipticity, and (ii) Tip-Tip (TT)- in this case the U nuclei approach along their major axes and the overlap region is circular and has smaller  $\varepsilon_2$  as compared to the BB configuration [25]. While both the configurations have similar  $N_{part}$ ,  $N_{coll}$  is larger by a factor  $\sim 1.3$  in the case of TT events as compared to BB. Thus the two component scheme as given by Eq. 4 predicts that the highest multiplicity U+U events must be from TT configurations with smaller  $v_2$  due to circular shape of the collision zone. As discussed earlier this leads to the prediction of a knee-like structure in the centrality variation of  $v_2$  as well as a strong anti-correlation of  $v_2$  vs multiplicity in the top ZDC events, unlike what is seen in experiments.

The  $\varepsilon_2$  calculated within the ambit of MCGM and shMCGM have been used to obtain  $v_2$  through the scaling  $v_2 = \kappa \varepsilon_2$  with  $\kappa \sim 0.2$  [26]. In Fig.3, we have compared the centrality dependence of this scaled  $\varepsilon_2$  with the STAR data on  $v_2\{2\}$  in U+U collisions [12]. We find a

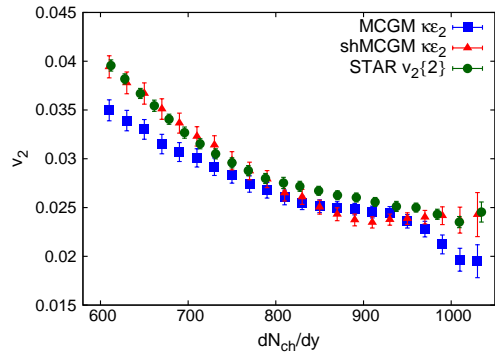


FIG. 3. The centrality dependence of  $v_2$  for U+U at  $\sqrt{s_{NN}} = 193$  GeV as obtained in MCGM and shMCGM. The experimental data is from Ref. [12].

fairly good qualitative agreement between data and shMCGM. The most striking difference between shMCGM and MCGM occurs for the most central events where the effect of shadow is expected to be the highest. Clearly, the knee-like structure that is predicted by the MCGM (but not observed in data) is washed away in the case of shMCGM which accurately follows the data. The knee like structure has vanished because the effect of shadowing moderates the collision process to bring a balance in the effective numbers of collisions for tip-tip and body-body geometry by reducing  $N_{coll}$  more in TT compared to BB configurations.

Another interesting point to note from Fig. 3 is that  $\varepsilon_2$  in case of shMCGM is higher as compared to MCGM. In a typical mid-central collision where  $\varepsilon_2$  is generated mainly because of the elliptical shape of the overlapped region, the ends of the major (minor) axis of the elliptical overlap region receive contribution from the boundary region of both (one) nucleus. Hence there is lesser (higher) energy deposition. Now as seen in Eqs. 18 and 19, the effect of shadow is weaker (stronger) where lesser (more) nucleons are expected to deposit energy. This leads to milder (stronger) shadowing effect at the ends of the major (minor) axis, which effectively enhances the ellipticity in shMCGM compared to MCGM. Similar arguments also show that models based on gluon saturation physics are expected to generate higher  $\varepsilon_2$  as compared to MCGM [27].

The high multiplicity events have been looked at in yet another way- by applying cuts on the ZDC. Top (0–0.1)% and (0–1)% ZDC events have been analyzed in STAR [12]. The MCGM predicts a strong anti-correlation between  $v_2(\kappa\varepsilon_2)$  and multiplicity in these events. However, such strong anti-correlation was not seen in experiments as well as in the IP-Glasma model [17]. Here, we find that the new phenomenological parameter  $\lambda$  which encapsulates the nucleon shadowing effect could be suitably tuned in the shMCGM to agree

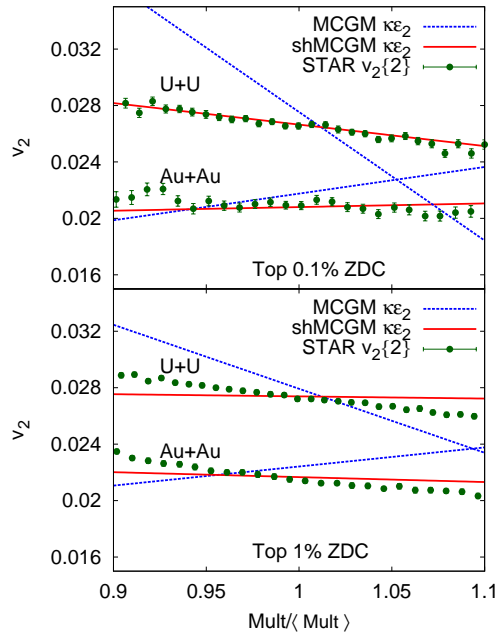


FIG. 4. Scaled  $\varepsilon_2$  vs multiplicity plot for U+U at  $\sqrt{s_{NN}} = 193$  GeV and Au+Au at  $\sqrt{s_{NN}} = 200$  GeV for top ZDC events as obtained in MCGM and shMCGM. The experimental data is from Ref. [12].

with data. For the same value of  $\lambda$ , a much improved agreement is seen between data and shMCGM in Fig. 4 for both collision systems, U+U and Au+Au.

We finally turn our attention towards E/E distribution of  $\varepsilon_2$ . It has already been pointed out that the E/E distribution of  $\varepsilon_2$  in dynamical models is narrower than that of MCGM [10, 11, 17]. We noted earlier in Eq. 20 that the shadow suppresses both  $N_{part}$  and  $N_{coll}$  as well as their fluctuations. This suggests that E/E fluctuation of other observables computed in the shMCGM should be narrower compared to the MCGM. In Fig. 5 we have plotted the E/E distribution of  $\varepsilon_2/\langle\varepsilon_2\rangle$  for U+U and Au+Au collisions for (20–30)% centrality. The E/E distribution from the shMCGM is indeed narrower compared to the MCGM case and compares well with the IP-Glasma distribution. Thus, overall we find the shMCGM to provide ICs for U+U at  $\sqrt{s_{NN}} = 193$  GeV and Au+Au at  $\sqrt{s_{NN}} = 200$  GeV that are in agreement with experimental data as well as with predictions from other dynamical models. It is interesting to note that the results of shMCGM are in good agreement with data for Pb+Pb collisions at  $\sqrt{s_{NN}} = 2.76$  TeV [28].

Finally to conclude, MCGM has been employed routinely in the study of HICs to ascertain ICs, based on

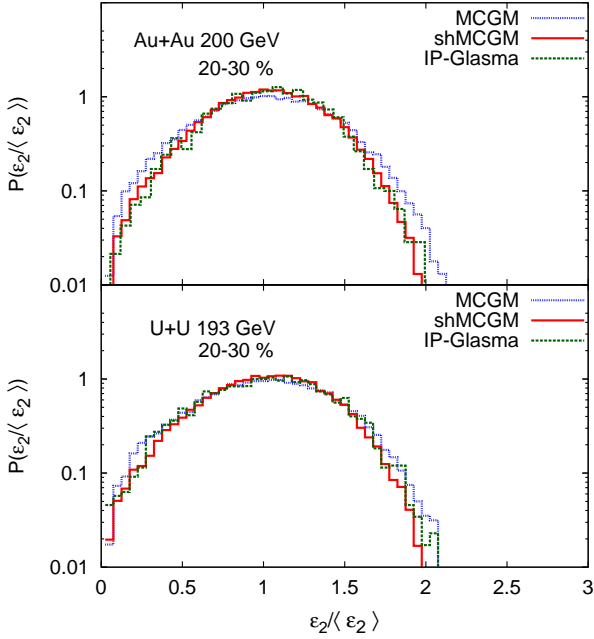


FIG. 5. The event by event probability distribution of  $\varepsilon_2$  for U+U at  $\sqrt{s_{NN}} = 193$  GeV and Au+Au at  $\sqrt{s_{NN}} = 200$  GeV for (20 – 30)% centrality events as obtained in MCGM and shMCGM. The IP-Glasma data is from Ref. [17].

geometric considerations and a few free parameters that are extracted from fits to data. However, lately it has been superseded by the QCD based models of ICs. The

high multiplicity U+U events and the data on E/E flow distributions at the LHC have clearly ruled out the simple geometrical MCGM in favour of the latter models. Here we explored the possibility of bridging the above gap by including the effect of shadowing due to leading nucleons in the MCGM, an idea that dates back to 1950s [22] but rarely explored in HICs. In the conventional MCGM, all the sources are given equal weightage to deposit energy. In the shMCGM, leading sources are given a larger weightage than those in the interior. For a suitable choice of the shadow parameter, we find good agreement between data and shMCGM. We also argue that the presence of shadow in the shMCGM invariably reduces the E/E fluctuation as compared to the conventional MCGM. Thus, we now find good agreement between IP-Glasma and shMCGM predictions of the E/E distribution of  $\varepsilon_2$ . Our study hints that incorporating shadowing in the MCGM could bring such geometrical models closer to dynamical models. At this point it is an interesting question to ask whether our ansatz for shadow given by Eq. 1 is unique or equally good description of the same observables is possible with other ansatz. In this regard it might be a worthy exercise to check whether on starting from a QCD based dynamical approach it is possible to derive an effective form of the shadowing factor and predict the shadow parameter  $\lambda$  in terms of the relevant scales of the problem rather than treating it as a free parameter.

*Acknowledgement:* We would like to thank Prithwish Tribedy for providing the IP-Glasma data. SC acknowledges him for many fruitful discussions on the initial condition and thanks “Centre for Nuclear Theory” [PIC XII-R&D-VEC-5.02.0500], Variable Energy Cyclotron Centre for support. SG and MH acknowledge Department of Atomic Energy, Govt. of India for support.

- 
- [1] H. Song, S. A. Bass, U. Heinz, T. Hirano, and C. Shen, Phys. Rev. Lett. **106**, 192301 (2011), [Erratum: Phys. Rev. Lett.109,139904(2012)].
  - [2] A. Bialas, M. Bleszynski, and W. Czyz, Nucl. Phys. **B111**, 461 (1976).
  - [3] D. Kharzeev and M. Nardi, Phys. Lett. **B507**, 121 (2001).
  - [4] M. L. Miller, K. Reygers, S. J. Sanders, and P. Steinberg, Ann. Rev. Nucl. Part. Sci. **57**, 205 (2007).
  - [5] W. Broniowski, M. Rybczynski, and P. Bozek, Comput. Phys. Commun. **180**, 69 (2009).
  - [6] K. J. Eskola, K. Kajantie, P. V. Ruuskanen, and K. Tuominen, Nucl. Phys. **B570**, 379 (2000).
  - [7] D. Kharzeev, E. Levin, and M. Nardi, Phys. Rev. **C71**, 054903 (2005).
  - [8] T. Hirano, U. W. Heinz, D. Kharzeev, R. Lacey, and Y. Nara, Phys. Lett. **B636**, 299 (2006).
  - [9] B. Schenke, P. Tribedy, and R. Venugopalan, Phys. Rev. Lett. **108**, 252301 (2012).
  - [10] C. Gale, S. Jeon, B. Schenke, P. Tribedy, and R. Venugopalan, Phys. Rev. Lett. **110**, 012302 (2013).
  - [11] H. Niemi, K. J. Eskola, and R. Paatelainen, (2015), arXiv:1505.02677 [hep-ph].
  - [12] L. Adamczyk et al. (STAR), (2015), arXiv:1505.07812 [nucl-ex].
  - [13] A. R. Timmins (ALICE), J. Phys. Conf. Ser. **446**, 012031 (2013).
  - [14] G. Aad et al. (ATLAS), JHEP **11**, 183 (2013).
  - [15] S. A. Voloshin, Phys. Rev. Lett. **105**, 172301 (2010).
  - [16] A. Goldschmidt, Z. Qiu, C. Shen, and U. Heinz, (2015), arXiv:1507.03910 [nucl-th].
  - [17] B. Schenke, P. Tribedy, and R. Venugopalan, Phys. Rev. **C89**, 064908 (2014).
  - [18] M. Rybczynski, W. Broniowski, and G. Stefanek, Phys. Rev. **C87**, 044908 (2013).
  - [19] S. Eremín and S. Voloshin, Phys. Rev. **C67**, 064905 (2003).
  - [20] S. S. Adler et al. (PHENIX),

- Phys. Rev. **C89**, 044905 (2014).
- [21] J. S. Moreland, J. E. Bernhard, and S. A. Bass, Phys. Rev. **C92**, 011901 (2015).
- [22] R. J. Glauber, Phys. Rev. **100**, 242 (1955).
- [23] A. Bzdak, Phys. Lett. **B647**, 358 (2007), arXiv:nucl-th/0611085 [nucl-th].
- [24] P. Bozek and W. Broniowski, Phys. Rev. **C88**, 014903 (2013).
- [25] M. R. Haque, Z.-W. Lin, and B. Mohanty, Phys. Rev. **C85**, 034905 (2012).
- [26] P. F. Kolb, J. Sollfrank, and U. W. Heinz, Phys. Rev. **C62**, 054909 (2000).
- [27] H.-J. Drescher, A. Dumitru, A. Hayashigaki, and Y. Nara, Phys. Rev. **C74**, 044905 (2006).
- [28] S. Ghosh, S. K. Singh, S. Chatterjee, J. Alam, and S. Sarkar, (2016), arXiv:1601.03971 [nucl-th].